Space-time gravity variations to look deep into the southern flank of Etna volcano

Filippo Greco[(1)], Gilda Currenti[(1)], Ciro Del Negro[(1)], Rosalba Napoli[(1)], Danila Scandura[(1,2)], Gennaro Budetta[(1)], Maurizio Fedi[(3)], Enzo Boschi[(1)]

[(1)] *Istituto Nazionale di Geofisica e Vulcanologia, Sezione di Catania, Italy*

[(2)] *Dipartimento di Matematica e Informatica, Università di Catania, Italy*

[(3)] *Dipartimento di Scienze Della Terra, Università degli Studi di Napoli "Federico II",Italy*

Abstract

A microgravity 14-year-long data set (October 1994 - September 2007) recorded along a 24-kilometer East-West trending profile of 19 stations was analyzed to detect underground mass redistributions related to the volcanic activity involving the southern flank of Mt Etna volcano (Italy). A multiresolution wavelet analysis was applied to separate the volcano-related signal from the unwanted components due to mainly instrumental, human-made and seasonal effects. The residual space-time image evidenced two complete gravity increase/decrease cycles mainly affecting the central and eastern stations of the profile. The first gravity increase (early-1995 to end-1996) – decrease (end-1996 to late-1998) cycle reached a maximum amplitude of approximately 90 μGal. The second gravity increase (mid-1999 to mid-2000) – decrease (mid-2000 to early-2004) cycle attained an amplitude of about 80 μGal peak-to-peak. After about five years of a persistent negative gravity anomaly, a new semi-cycle started at the end of 2006 and continued during the last survey carried out in September 2007. We modeled the 1994-2007 gravity anomalies using a Quadratic Programming algorithm to infer the position and the evolution of the sources beneath the profile. The computed positive mass variations of about 1.05 x 10^{11} kg were interpreted as magma accumulation, while negative mass changes of about -1.20 x 10^{11} kg could reflect either magma migration or opening of new voids by tectonic tensile stresses within a source volume, where tensional earthquakes occurred.

Keywords: Microgravity, Volcano monitoring, Etna volcano

Introduction

Temporal gravity variations in active volcanic areas are related to a wide set of geophysical phenomena (i.e. sub-surface mass-redistributions due to volcanic processes, surface elevation changes, seismicity, etc.), and their amplitude, wavelength and duration depend on several parameters such as size, depth and evolution rate of the sources. The observed gravity changes range in amplitude between a few μGal and several hundred μGal with a spectrum varying from 1 second to more than 1 year [*Hinderer and Crossley*, 2000; *Greco et al.,* 2008]. Over the past few decades, we have been intensively monitoring the gravity field on Mt Etna, and several time changes of the gravity field associated with subsurface mass redistributions driven by magmatic processes were detected [*Budetta and Carbone*, 1998; *Budetta et al.*, 1999, *Branca et al.*, 2003; *Carbone et al.*, 2003a; 2003b, *Bonforte et al.*, 2007; *Carbone and Greco*, 2007; *Currenti et al.,* 2007].

Microgravity studies at Etna have become an effective volcano monitoring tool because of long records of regular observations. Discrete microgravity observations have been routinely performed at Etna since 1986 [*Budetta et al.*, 1989; *Budetta and Carbone*, 1998]. We present and discuss a 14-year-long gravity data set recorded between October 1994 and September 2007 period, along a 24-kilometer East-West trending profile of 19 stations on the southern slope of the volcano running from Zafferana (525 m a.s.l.) to Adrano (590 m a.s.l.) across the Rifugio Sapienza (1890 m a.s.l., Fig. 1). Approximately, quasi-monthly measurements along the East-West profile have been usually conducted (up to weekly during periods of eruptive crises). During this period, the Etna eruptive activity was confined to the summit area (mid-1995 to mid-2001), where lava flows, lava fountains and intense explosive events occurred in rapid succession at the four summit craters and nearby vents [*Allard et al.*, 2006]. The period 2001 – 2006 was also marked by two flank eruptions in 2001 and 2002-2003, which showed simultaneous central-lateral and eccentric activity [*Behncke and Neri*, 2003], by a passive flank effusion in 2004-2005 and by the 2006 eruption, characterized by strong degassing from the uppermost vent with strong Strombolian activity.

In this paper we focus on repeated gravity measurements along the East-West profile to investigate the interaction between the long-term volcano eruptive behaviors and the dynamic processes of the Etna volcano. In particular we study the southern sector of the volcano, which plays a key role in regulating the magma rising from the upper mantle to the shallower plumbing zone.

Data presentation and analysis

The East-West profile, because of the more frequent measurements and the high station density (almost 1 station/km), provides the core microgravity data for Etna (the time resolution of sequences recorded in other sectors of the volcano are not as frequent as that from the East-West profile). Since its installation (summer of 1994), 96 surveys were carried out and a large data-set, spanning a 14-year long period (1994-2007), was collected using the Scintrex CG-3M gravimeter (serial # 9310234).

The measurements along this profile were carried out by the “step method”, thus each couple of adjacent stations is connected at least three times in order to monitor continuously the instrumental performance. All measurements were then referred to the outermost station of the profile (Adrano, Fig. 1), since it is the least likely station to be affected by volcanically-induced gravity changes [*Budetta et al.*, 1999]. The instrumental error on temporal gravity differences along the East-West profile is about 10 μGal [*Budetta and Carbone*, 1997; *Carbone et al.*, 2003b]. During each survey, the Scintrex CG-3M gravimeter was calibrated along the Catania – Enna calibration line [*Budetta and Carbone*, 1997].

Figure 2 shows the gravity variations measured in the East-West profile stations (y axis) between October 1994 and September 2007 (x axis). The space-time map shows significant gravity increase/decrease cycles, with different wavelengths, reaching the maximum amplitude of approximately 110 μGal. The main gravity cycles are concentrated along the central and eastern limb of the profile, where almost all the gravity stations are close or coincident with GPS benchmarks. Since ground deformation during the 1994-2007 period does not show vertical variations able to produce significant gravity changes in the zone covered by the gravity profile, the

gravity data-set was not corrected for the free-air effect. Indeed, the height variations have been within 2-4 cm [*Puglisi and Bonforte*, 2004; *Palano et al.*, 2007; *Bonforte et al.*, 2008], which give gravity variations within 6-12 μGal, assuming a free air gradient of –308 μGal m^{-1}. Thus, the free-air effect is negligible compared with the observed gravity changes and with the uncertainty of ±10 μGal affecting the East-West profile data [*Budetta et al.,* 1999; *Carbone et al.,* 2003b]. Besides useful signal (i.e. the volcano-related one), the gravity map includes unwanted components (instrumental, human-made, seasonal and other kinds of noise). In order to filter the gravity data-set from these last components the wavelet multi-resolution analysis was applied. The wavelet analysis provides a good separation of the long period component from the short period one, and allows exploring the local features of the signal with a detail matched to their characteristic scale. Using the discrete wavelet transform (DWT), the gravity data are decomposed into a low-resolution approximation level and several detail levels [*Fedi and Quarta*, 1998; *Fedi and Florio*, 2003]. The detail levels can be regarded as the difference of information between the approximations of the signal at subsequent scales. In a two-dimensional multiresolution process three detail levels can be obtained along horizontal, vertical and diagonal directions at each scale [*Fedi and Florio*, 2003]. We are particularly interested in the horizontal and vertical components that reflect temporal and spatial gravity variations, respectively. The space-time matrix consists of 50 x 100 grid data at about 500 m step and with a 1.5 month average sampling. The multiresolution analysis decomposes the data from the finest to the coarsest levels, corresponding to level $\ell = -(L-1)$ and $\ell = 0$, respectively, where $L = \log_2(m)$ for discrete data of m values. In the case of a 2D multiresolution analysis m is the minimum size of the data matrix dimension. For the considered gravity data-set the finest level is at most $\ell = -5$.

Several wavelet bases may be, however, taken into consideration to compute the DWT. The ‘‘Minimum Entropy Criterion” (MEC) was used to evaluate a compactness measure, which estimates how the signal energy can be substantially assembled in few components [*Coifman and Wickerhauser*, 1993; *Fedi and Quarta*, 1998]. Using this criterion, the entropy of the wavelet coefficients for various types of wavelet basis may be determined, and the optimal wavelet basis may be chosen as the one giving the minimum entropy value. The Shannon’s entropy was

calculated for several wavelet basis over the wavelet coefficients from level $\ell = 0$ to $\ell = -5$, and ranges between 3.14 and 4.50 (Table 1), with the minimum value obtained for the Symlet 4 basis. The wavelet decomposition of gravity data set by Symlet 4 gives one low-resolution approximation map and five total detail maps with the most energetic levels from $\ell = -1$ to $\ell = -5$ (Fig. 3).

The D_{-5} detail map (Fig. 3) evidences the presence of local noise at VE and TG stations situated at the central part of the profile, very close to the Rifugio Sapienza (Fig. 1). Indeed, these stations are often affected by a human-made noise due to the presence of tourist facilities. The high resolution map of the D_{-4} detail shows up short-wavelength time-space gravity variations (Fig. 3). Most of the signal in the horizontal components of the D_{-4} detail map can be associated to quite shallow sources which produce localized gravity anomaly. Besides the presence of high frequency components in the horizontal details, seasonal variations come up in the vertical details of the D_{-4} and D_{-3} maps (Fig. 3). A late-winter maximum and a late-summer minimum is observed with amplitude ranges between ± 40 μGal peak-to-peak in the easternmost stations of the profile. These gravity changes are consistent with water-table fluctuations. A gravity change of about ± 20 μGal, corresponding to water-table fluctuations of 3.5 - 5 m and an effective porosity of the aquifer in the range 0.09 to 0.14 [*Aureli*, 1973], was evaluated by *Budetta et al.* [1999] using average values estimated from only the western stations data (from CH to TG; Fig. 1). The DWT analysis evidences that seasonal variations induce local effects at each gravity station. Different fluctuations in the underground water-table depend on climate, weather, and geological setting around the gravity station and the related gravity effect can differ from station to station in magnitude and temporal dependence. Higher gravity variations are observed on the eastern part. Indeed, yearly rainfall data show high precipitation value on the eastern flank with a precipitation ratio of about two with respect to the westernmost flank [*SIAS*, 2007]. In addition, the stations located in the westernmost tip of the profile are very close to the extended outcrops of the sedimentary substrate [*Romano*, 1982]. The substrate serves as a seal along the base of the fractured and vesicular volcanic sequence, and hence the Etna's aquifers are confined mostly to volcanic rock [*Ogniben*, 1966]. Accordingly, only restricted aquifers are located near the westernmost stations (Fig. 1), where any gravity change due to water-table fluctuations can be then considered meaningless.

Once the wavelet analysis was performed and gravity data were suitably filtered from the (i) noise (D_{-5}), (ii) the effect of sources very close to the surface (D_{-4}), and (iii) seasonal components due to water-table fluctuations (D_{-3} and D_{-4}), the gravity residual can be attributed to subsurface bulk density (Fig. 4). Since the vertical components D_{-3} and D_{-4} contain gravity variations with a period of about one year, the filtering procedure unfortunately could remove useful signal with similar temporal scale. Thus, in the following we consider only gravity variations with period longer than one year.

The residual gravity map shows long period gravity increase and decrease cycles with duration ranges between a few years and several years, and with a wavelength of order of 10-12 km (Fig. 4). The gravity increase/decrease cycles affect mainly the central and eastern stations of the profile, whereas the gravity changes at stations closest to the reference station (ADR) remain within 20 μGal during the entire period (Fig. 4).

A first complete gravity increase/decrease cycle attains a maximum amplitude of approximately 90 μGal, which started during the early months of 1995 (gravity increase), culminated at the end of 1996, and continued until late-1998 (gravity decrease), when the mean value of gravity at each station reached a level lower than it was in 1994-95, before the increase took place (Fig. 4). The considerable increase/decrease of gravity field recorded in this period (late-1995 to late-1998) is among the largest ever recorded along the profile until now.

A second increase/decrease gravity cycle, affecting the same stations of the previous one, but mostly evident in the central portion of the profile, was observed between mid-1999 (gravity increase), culminating at the mid-2000 (maximum amplitude about 80 μGal) and continuing until early-2004. The 1999-2000 gravity increase was interrupted by a progressive gravity decrease of about 80 μGal, which started between early-2001, continued very slowly until early-2004, and partially compensated for the previous gravity increase. After the 2001 no significant gravity increase/decrease cycles, in terms of both amplitude and wavelength, occurred. Moreover, the gravity field on the easternmost stations shows a persistent negative gravity anomaly during the period 2001-2006, whereas the gravity in the western flank is almost unchanged. After about 5 years of absence of significant gravity cycles, a new semi-cycle with characteristics similar to the

previous ones seems to start at the end of 2006 and continues during the survey carried out in September 2007.

Density model and volcanological evidences

Since the gravity observations are collected along a profile, we accomplished a 2D density model. Even if this assumption is an overly simplification of the volcano edifice, it somehow allows for obtaining a rough estimate of the gravity source depths. We performed a gravity inversion to have hints about the gain/loss of mass over time on the subsurface beneath the gravity stations. We modeled the subsurface in a set of infinitely long rectangular prisms with uniform densities ρ_1 ,….., ρ_m. In order to allow the maximum flexibility and represent realistic geological structures, the domain extends 25 km for taking into account the side effect of source bodies surrounding the observational area. It is subdivided into a set of rectangular prisms of 0.5 x 0.5 km in size below sea level and of 0.25 x 0.25 km above sea level in order to better approximate the topography. The bottom of the domain was assumed to be 8 km b.s.l. on the basis of the depth resolution (about 7-8 km) due to the extension of the gravity profile. Applying this numerical approach, the gravity field at the i-*th* observation point is computed by:

$$G_i = \sum_{j=1}^{m} \rho_j a_{ij} \qquad (1)$$

where a_{ij} elements quantify the contribution to the gravity anomaly at i-*th* observation point due to the density ρ of the j-*th* prism [*Blakely*, 1995]. The inverse problem can be formulated as an optimization problem [*Napoli et al.*, 2007] aimed at finding the unknown density values **x** that minimize a data misfit ϕ_d and a smoothing functional ϕ_r, defined as:

$$\phi = \phi_d + \lambda \phi_r = \frac{1}{2}\left[\left(\mathbf{G} - \mathbf{G}_{obs}\right)^T \left(\mathbf{G} - \mathbf{G}_{obs}\right)\right] + \lambda \phi_r \qquad (2)$$

where λ is a regularization parameter, namely a trade-off between minimizing a measure of the data misfit ϕ_d and a smoothing functional ϕ_r. Because of the lack of depth resolution in the modeling procedure [*Fedi and Rapolla*, 1999], when the inversion is performed to minimize the functional in (Eq. 2), the density solution **x** is concentrated close to the observation points. To avoid this

problem, the smoothing functional is defined in a way to give sources at different depths equal probability to enter in the solution. A depth weighting function is introduced [*Li and Oldenburg*, 1996] that leads to the following functional:

$$\phi = \frac{1}{2}\left[(\mathbf{G}-\mathbf{G}_{obs})^T(\mathbf{G}-\mathbf{G}_{obs})\right] + \lambda(\mathbf{x}-\mathbf{x_0})^T\mathbf{W}^T\mathbf{W}(\mathbf{x}-\mathbf{x_0}) \qquad (3)$$

where **W** is a diagonal weighting matrix, whose elements are the weights associated to the prisms [*Li and Oldenburg*, 1996]. It takes into account that the gravity field decays as inverse distance. The elements of the **W** matrix are the gravity field values due to a prismatic source under the observation point. The depth weighting values are then normalized, so that the maximum value is unity. To ensure that the solution is geologically reasonable, it is advisable to assign realistic bounds on the density values to avoid abnormal solution in the model. The minimization of the quadratic functional in Eq. (3) subjected to bound constraints is solved using a Quadratic Programming algorithm based on an active set strategy [*Gill et al.*, 1991]:

$$min\,\phi = min\left[\frac{1}{2}\mathbf{x}^T\mathbf{Q}\mathbf{x} - \mathbf{d}^T\mathbf{x}\right], \quad \mathbf{L} \le \mathbf{x} \le \mathbf{U} \qquad (4)$$

where $\mathbf{Q} = \mathbf{A}^T\mathbf{A} + \lambda\mathbf{W}^T\mathbf{W}$ and $\mathbf{d} = \mathbf{A}^T\mathbf{T} + \lambda\mathbf{W}^T\mathbf{W}\mathbf{x_0}$, **L** and **U** are the vectors of lower and upper bounds of density values and $\mathbf{x_0}$ is the initial value. We allow the solution to vary in a wide range $\pm$ 0.5 kg/m^3. The quadratic formulation of the problem is solved iteratively by generating a sequence of feasible solutions that converge toward the optimal solution. The iteration is stopped when no relative improvements in the functional are achieved.

Among the several techniques that have been developed to properly estimate λ in ill-posed inverse problem, we used the L-curve criterion to find a trade-off between minimizing the data misfit ϕ_d and the smoothing functional ϕ_r [*Farquharson and Oldenburg*, 2004; *Fedi et al.,* 2005]. A family of solutions is achieved by varying λ from 0 to ∞ and the data misfit ϕ_d of the regularized solutions is plotted versus the corresponding smoothing functional ϕ_r (Fig. 5). In the horizontal part of the L-curve (data misfit constant), the smoothing functional ϕ_r increases rapidly without much decreasing the data misfit ϕ_d. In the vertical part of the L-curve (smoothing functional constant), the data misfit

ϕ_d increases without reducing the smoothing functional ϕ_r. The λ value in correspondence of the point of maximum curvature represents a compromise between minimizing the data misfit ϕ_d and the smoothing functional ϕ_r [*Farquharson and Oldenburg*, 2004]. Using the L-curve criterion, a value of λ = 500 is achieved (Fig. 5). The inversion solution achieved at time *t* is used as initial value $\mathbf{x_0}$ in the inversion at the next time step *t+1* in a way to assure the continuity of the density variations. The computed gravity anomaly is shown in Figure 6a and agrees well with the observed field. The residual field (Fig. 6b) has a null mean and a standard deviation of 3.67 μGal. However, short-wavelength residuals less than 20 μGal remain along the central and eastern portions of the profile (Fig. 6b).

Figure 7 shows the retrieved mass per unit length of the prisms at three different depths: (a) 1 km; (b) 3 km; (c) 6 km b.s.l. Although the modelling of the gravity anomalies is limited by the 2D model approximation, significant spatial and temporal increase/decrease density cycles can be recognized at different depths in the central and eastern parts of the profile (longitude ranges between about 492 km and about 508 km), while the westernmost part does not show significant density variations. In the shallow level, positive density anomalies were observed in the easternmost part affecting almost the whole time interval of observation. Since their marginal position compared to the profile, these anomalies are not taken into account in our discussion.

The gravity model allows to quantify and discriminate in time and space if a gain or loss of mass occurs in the investigated volume (Fig. 7). By looking the 2D density distribution model at three different depths, we can draw the following evidences. The 1995-1997 high density deeper anomaly starts in the late summer 1995 when eruptive activity resumed at Etna summit area [*Armienti et al.*, 1996]. This density increase can be interpreted as deeper magma accumulation, which seems to successively migrate upward toward the central area of the profile. It could have supplied the continuous and persistent magmatic activity at the Southeast Crater (SEC) during 1998-1999 (Fig. 8a). Accordingly, ground deformation and seismic data evidenced an intrusive episode occurred along the NNW-SSE structure in January 1998, which yielded a shallow dike rising within the volcanic edifice [*Bonaccorso and Patanè*, 2001].

Since the end of 1999, another deep high-density anomaly extending down to the deep level is detected. It could have fed the activity of summit craters observed in 2000 [*La Delfa et al.*, 2001; *Corsaro and Pompilio*, 2004]. Compositional investigations on products erupted during the 2000 activity demonstrates that a primitive and volatile rich magma progressively entered into a storage zone between 3 and 5 km depth [*Corsaro et al.*, 2007]. The arrival of this primitive and volatile rich magma in plumbing system was fundamental for triggering the fire fountaining activity observed at SEC (Fig. 8a). This high density anomaly is evident until mid 2001 at 6 km depth and seems to move toward shallower depths until late 2002. It could be consistent with mass increases due to rapid injection of magma coming from deep storage system, feeding the 2001 eruption, as shown by petrologic evidences on erupted magma products [*Corsaro et al.*, 2007], and the 2002-2003 eruption occurred on the southern flank.

After the 2001 eruption no significant recharging phases are observed at 6 km depth and only a modest high density anomaly is detected at 1 km depth during the 2002-2003 eruption period. In the 2002-2006 time interval (encompassing 2003-2004 eruption) no significant high density anomalies are observed at 3 km and 6 km depths. Only a new slight high density anomaly is observed since the beginning of 2005 at shallow depths. The absence of ascent of new magma is also consistent with the compositional analysis carried out on the products emitted during the 2003-2004 eruptive events [*Corsaro and Miraglia*, 2004]. Both geophysical and petrologic data suggest that this eruption was not triggered by the intrusion of a new magma from depth, but it was fed by magma already stored in the shallow plumbing system after the activity of the SEC in 2000 and 2001 [*Corsaro and Miraglia*, 2004]. The purely effusive nature of this eruption, fed by a degassed resident magma, and the fracture dynamics suggest that magmatic overpressure played a limited role in this eruption. Rather, lateral spreading of Etna's eastern flank combined with general inflation of the edifice triggered a geodynamically controlled eruption [*Burton et al.*, 2005].

The Figure 7 highlights also the presence of a persistent low density anomaly in the eastern part of the profile (longitude ranges between about 500 km and about 508 km). This area extends down to a depth of 3 km and vanishes below a depth of 6 km. To interpret the low density anomalies, we hypothesize that rather than being only associated to the migration of the magma, the dynamic of

the southeastern sector of the volcano could be also involved. The eastern flank of Etna is characterized by frequent shallow seismic activity (depth ca. < 7 km) and by a seismic creep along some faults, interpreted as evidence of gravitational and/or magma-induced spreading of this large sector of the volcano [*Borgia et al.*, 1992; 2000; *Bousquet and Lanzafame*, 2004; *Tibaldi and Groppelli*, 2002; *Acocella et al.*, 2003; *Neri et al.*, 2005]. We compared the 2D density model with the hypocenter depths of seismic events occurred during September 1999 – December 2005 period in the latitude ranges between 4168 km and 4174 km (coordinates are expressed in UTM), covering the gravity profile (Fig. 1). The selected seismic events do not include earthquakes due to either the dynamic of NE-Rift or the summit craters activity but rather earthquakes linked to the dynamics of the upper and medium southern flank of the volcano. A correlation was found between the cluster of the selected seismic events ($M \geq 2.5$) and the low density anomalies at the average depth of 3 $\pm$1 km and 6 $\pm$1 km for all time interval considered, while the correlation at the average depth of 1 $\pm$1 km is negligible (Fig. 7). Shallow earthquakes (depth < 10 km) may be related to a progressive increase of the tectonic stress. At Etna a ca. NS strike-slip compressive stress regime coexist with a ca. ESE–WNW shallower tensile regime that favours the magma ascent through the shallow crust [*Patanè et al.*, 2003]. Indeed, the tectonic stress causes crack density increases in the brittle shallow layers and the volcanic pile. Moreover, Figure 7c shows up a cluster of seismic events at 6 km depth in correspondence of the high density anomaly during the 1999-2001 period. This is in agreement with the seismic interpretation that considers deepest earthquakes related to systematic magma refilling in the middle-upper crust from below [*Patanè et al.*, 2004].

We computed the mass temporal variations and discriminated between positive and negative values on the basis of prism density changes (Fig. 8c). Mass fluctuations can be interpreted in terms of emptying or filling of voids. Positive variations are related to gain of mass or density changes due to medium compressibility, whereas negative variations are interpreted as mass loss or opening of new cracks. In order to give an overall picture between the computed mass variations and the volcano eruptive patterns, we compared the long-term mass increase/decrease cycles (Fig. 8c) with a chronogram of the flank eruptions and the activity at the four summit craters of Mt Etna (Fig. 8a) and the cumulative eruptive volume (expressed as dense rock equivalent; Fig.

8b). This comparison shows that when new mass was gained beneath the profile (mid-1995 to mid-1998 and early-2000 to early-2002) intense and quasi-persistent activity at summit craters and lateral eruptions (2001 and 2002-2003) took place. The first recharging phase started in correspondence with the resumption of the summit activity (mid-1995), after a period of eruptive quiescence following the 1991-1993 eruption. The maximum negative mass per unity length is about -2.5 x 10^7 kg/m in mid-2004, while the maximum positive mass per unity length is 2.1 x 10^7 kg/m in late-1996 (Fig. 8c). If we consider an average prism length of 5 km, which is a reasonable approximation of the sources in the investigated area [*Bonforte and Puglisi*, 2003; *Carbone et al.*, 2003b], negative and positive mass changes of -1.20 x 10^{11} kg and 1.05 x 10^{11} kg are estimated, respectively. The cumulative erupted volume in the same period is 1.5 x 10^8 m^3 (Fig. 8b), which gives an erupted mass of 3.75 x 10^{11} kg assuming an average medium density of 2500 kg/m^3. The estimated mass decrease is comparable with the erupted one, although we have also to consider the contribute due to the opening of new cracks correlated with the occurrence of seismic events. The excess of erupted mass can occur since (a) the sampling rate is too low to detect fast magma rising, and/or (b) magma comes up through other pathways.

Discussion and Conclusions

The East-West profile is located in the southern flank of Etna, where local structural systems connected by regional lineaments play a key role in the dynamic processes of the volcano [*Bonaccorso and Patanè*, 2001; *Patanè and Privitera*, 2001]. Previous gravity investigations along this profile [*Budetta and Carbone*, 1998; *Budetta et al.*, 1999; *Carbone et al.*, 2003b; *Carbone et al.*, 2007] have already provided insights about the intrusive processes in an elongated volume, oriented NNW-SSE, which regulates the flux of magma from the deeper mantle source to the upper plumbing system of Etna [*Patane et al.*, 2004]. The NNW-SSE orientation of this source volume coincides with one of Etna's major structural trends, which is the preferred alignment for the ascent of Etnean magmas [*Ferrucci et al.*, 1993; *Bonaccorso et al.*, 1994; *Alparone et al.*, 1994; *Continisio et al.*, 1997; *Budetta and Carbone*, 1998]. The eruptions of the past 30 years seem to be

mainly related to magma rising on the two NNW and NE primary structural trends [*Bonaccorso et al.*, 1996; *Bonaccorso and Patanè*, 2001; *Patanè and Privitera*, 2001].

As evidenced in the 2D model (Fig. 7), increase/decrease density cycles were observed in the central and eastern sectors of the profile during 1994-2007 period. In agreement with volcanological and geophysical evidences, the high density anomalies evidenced at 3 km and 6 km beneath the surface could reflect mass accumulations into the shallow magma storage source identified seismically at 5 ± 2 km depth b.s.l. [*Murru et al.*, 1999] and by GPS data at 5.7 – 6.5 km depth b.s.l. [*Houlié et al.*, 2006; *Palano et al.*, 2007; *Bonforte et al.*, 2008]. This magma storage source is located in the upper limit of the high-velocity body (HVB) detected from seismic tomography [*Chiarabba et al.,* 1999] and also evidenced through a 3D inversion of gravimetric data [*Schiavone and Loddo*, 2007]. The magma would prevalently rise along the western and northwestern border of the HVB, where two main NNW-SSE and NE-SW tectonic structures intersect and structural weaknesses develop between the HVB and surrounding rocks [*Patanè et al.*, 2003]. Conversely, the low density anomalies observed at different depths (Fig. 7; late-1997 to late-1999 and early-2001 to mid-2006 periods), rather than being merely associated only to the underground magma drainage, could reflect also the passive mechanical response of the eastern to southern flanks of the volcano to tectonic stresses leading to a bulk density decrease. Accordingly, seismic data highlighted a progressive renewal of tensile stresses during the first months of 2001 with hundreds of events clustering on the southeastern sector of the volcano, mainly along a NNW-SSE alignment at a depth of 1 – 5 km, which coincides with the inferred low density anomalies [*Bonaccorso et al.*, 2004]. The instability of the eastern and southern flanks of the volcano is recognized as one of the main dynamic processes on Etna [*Borgia et al.*, 2000; *Neri et al.*, 2004; *Rust et al.*, 2005] and has been emphasized to be a triggering mechanism for some of the recent flank eruptions [*Acocella and Neri*, 2003; *Acocella et al.*, 2003; *Branca et al.*, 2003; *Burton et al.*, 2005]. Recurrences in temporal density changes highlight the occurrence of phenomena that lead magma ascent to shallower plumbing system and phenomena that guide contemporary magma drainage and seismic events. It is difficult to infer which kind of causal relationships exists between the mechanisms leading these cycles. For example, magmatic

overpressure below the volcano due to magma accumulation could be responsible for triggering the seismicity and the flank spreading and/or vice versa.

After the 2001 and 2002-2003 eruptions no significant high density anomalies were evidenced at 3 km and 6 km depths. Conversely, intense low density anomalies were observed after both these eruptions in the easterner sector of the profile in the shallower layers (Fig. 7). Ground deformation suggests that the eccentric dike intrusions accompanying the 2001 and 2002 lateral eruptions induced an exceptional acceleration of the sliding of the unstable eastern flank of the volcano [*Bonforte et al.*, 2008]. Moreover, the magma storage zone responsible for the high density anomalies was drained during the 2001 and 2002-2003 eruptions, as evidenced by petrologic studies [*Clocchiatti et al.*, 2004; *Mètrich et al.*, 2004], and could have been exhausted with the successive eruptions [*Allard et al.*, 2006].

The temporal correlation between the 2004-2005 and 2006 lateral eruptions with the occurrence of low density anomaly (no recharging phase occurred in this period) could indicate that magma accumulated previously was erupted, accordingly to *Burton et al.* [2005] and *Corsaro and Miraglia* [2004], or a different storage area not detectable by the East–West gravity profile was involved.

Finally, the analysis of long-period microgravity observations demonstrated that in the last 14 years just two (mid-1995 to mid-1998 and late-1999 to late-2001) major episodes of magma intrusion occurred beneath the southern sector of the volcano in the shallow storage zone (Fig. 7). Another mass accumulation in the shallow plumbing system of the volcano started in late 2006 and was still in progress in September 2007. We are confident that the frequent and regular surveys of the East-West gravity profile indicate possible magma rising months to years before the onset of a new Etna's eruption.

ACKNOWLEDGMENTS

This work was developed in the frame of the Division of Gravity and Magnetism at INGV-CT. The study was undertaken with financial support from the V3-LAVA and V4-FLANK projects (DPC-INGV 2007–2009 contract). We are grateful to SIAS (Regione Siciliana) for providing the rainfall data and the VOLUME project (European Commission FP6-2004-Global-3) for the seismic

database. We thank the Associate Editor Rodolfo Console and two anonymous reviewers for their useful comments that improved the manuscript.

References

Acocella, V., B. Behncke, M. Neri, and S. D'Amico (2003), Link between major flank slip and eruptions at Mt. Etna (Italy), *Geoph. Res. Lett. 30*, 24, 2286, doi:10.1029/2003GL018642.

Acocella, V., and M. Neri (2003), What controls flank eruptions?: the 2001 Etna eruption and the possible triggering mechanisms, *Bull. Volcanol. 65*, 517-529, doi: 10.1007/s00445-003-0280-3.

Allard, P., B. Behncke, S. D'Amico, M. Neri and S. Gambino (2006), Mount Etna 1993–2005: Anatomy of an evolving eruptive cycle, *Earth Sci. Rev. 78*, 85–114.

Alparone, S., O. Pellicori, A. Ursino, F. Ferrucci, S. Gresta, and I. Guerra (1994), Shallow microseismic swarms and intrusive mechanisms at Mt. Etna, *Acta Vulcanol. 4*, 75-79.

Armienti, P., M. D'Orazio, F. Innocenti, S. Tonarini, and L. Villari (1996), October 1995-February 1996 Mt Etna explosive activity: trace element and isotopic constraints on the feeding system, *Acta Vulcanol. 8*, 1-6.

Aureli, A. (1973), Idrogeologia del fianco occidentale etneo, in *2° Convegno Internazionale sulle Acque Sotterranee (Palermo)*, pp 425-486.

Behncke, B., and M. Neri (2003), Cycles and trends in the recent eruptive behaviour of Mount Etna (Italy), *Canadian J. Earth Sci. 40*, 1405-1411, doi: 10.1139/E03-052.

Blakely, R.J. (1995), Potential Theory in Gravity and Magnetic Applications, Cambridge University Press, New York, 435 pp.

Bonaccorso, A., F. Ferrucci, D. Patanè, and L. Villari (1996), Fast deformation processes and eruptive activity at Mt. Etna (Italy), *J. Geophys. Res. 101*, B8, 17467-17480.

Bonaccorso, A., R. Velardita, and L. Villari (1994), Ground deformation modelling of geodynamic activity associated with the 1991-1993 Etna eruption, *Acta Vulcanol. 4*, 87-96.

Bonaccorso, A. and D. Patanè (2001), Shear response to an intrusive episode at Mt. Etna volcano (January 1998) inferred through seismic and tilt data, *Tectonophysics 334/2*, 61-75.

Bonaccorso, A., A. Bonforte, F. Guglielmino, M. Palano and G. Puglisi (2006), Composite ground deformation pattern forerunning the 2004–2005 Mount Etna eruption, *J. Geophys. Res.111*, B12, doi:10.1029/2005JB004206.

Bonaccorso, A., S. D'Amico, M. Mattia and D. Patanè (2004), Intrusive mechanism at Mt Etna forerunning the July-August 2001 eruption, *Pure Appl. Geophys. 161*, 7, 1469-1487.

Bonforte, A., and G. Puglisi, 2003, Magma uprising and flank dynamics on Mount Etna volcano, studied using GPS data (1994–1995), *J. Geoph. Res.,108*, B3, 2153, 10.1029/2002JB001845.

Bonforte, A., A. Bonaccorso, F. Guglielmino, M. Palano, and G. Puglisi (2008), Feeding system and magma storage beneath Mt. Etna as revealed by recent inflation/deflation cycles, *J. Geophys. Res*., 113, B05406, doi:10.1029/2007JB005334.

Bonforte, A., F. Guglielmino, M. Palano, and G. Puglisi (2004), A syn-eruptive ground deformation episode measured by GPS, during the 2001 eruption on the upper southern flank of Mt Etna, *Bull. Volcanol. 66*, 4, 366-341.

Borgia, A., R. Lanari, E. Sansosti, M. Tesauro, P. Berardino, G. Fornaro, M. Neri and J.B. Murray (2000), Actively growing anticlines beneath Catania from the distal motion of Mount Etna's decollement measured by SAR interferometry and GPS, *Geophys. Res. Lett. 27*, 20, 3409-3412.

Borgia, A., L. Ferrari, and G. Pasquarè (1992), Importance of gravitational spreading in the tectonic and volcanic evolution of Mount Etna, *Nature 357*, 231-235.

Bousquet, J. C., and G. Lanzafame (2004), The tectonics and geodynamics of Mt. Etna: synthesis and interpretation of geological and geophysical data, in *Etna Volcano Laboratory*, *Geophys. Monogr. Ser., vol. 143*, edited by A. Bonaccorso, S. Calvari, M. Coltelli, C. Del Negro and S. Falsaperla, pp. 29-47, AGU, Washington, D. C.

Branca, S., D. Carbone, and F. Greco (2003), Intrusive mechanism of the 2002 NE-Rift eruption at Mt. Etna (Italy) inferred through continuous microgravity data and volcanological evidences, *Geoph. Res. Lett. 30 (20)*, 2077, doi:10.1029/2003GL018250.

Budetta, G., and D. Carbone (1997), Potential application of the Scintrex CG-3M grivimeter for monitoring volcanic activity: results of field trials on Mt. Etna, Sicily, *J. Volc. Geoth. Res. 76*, 199-214, 1997.

Budetta, G., and D. Carbone (1998), Temporal variations in gravity at Mt Etna (Italy) associated with the 1989 and 1991 eruptions, *Bull. Volcanol*. *59*, 311-326.

Budetta, G., D. Carbone, and F. Greco (1999), Subsurface mass redistributions at Mount Etna (Italy) during the 1995-96 explosive activity detected by microgravity studies, *Geoph. J. Int*. *138*, 77-88.

Budetta, G., M. Grimaldi, and G. Luongo (1989), Variazioni di gravità nell'area etnea (1986-1989), *Boll. GNV 5*, 137-146.

Burton, M.R., M. Neri, D. Andronico, S. Branca, T. Caltabiano, S. Calvari, R.A. Corsaro, P. Del Carlo, G. Lanzafame, L. Lodato, L. Miraglia, G. Salerno, and L. Spampinato (2005), Etna 2004–2005: An archetype for geodynamically-controlled effusive eruptions, *Geoph., Res., Lett.*, *32*, L09303, doi:10.1029/2005GL022527.

Carbone, D., Budetta, G. and F. Greco (2003a), Possible mechanisms of magma redistribution under Mt Etna during the 1994–1999 period detected through microgravity measurements, *Geoph. J. Int. 152*, 1–14.

Carbone, D., G. Budetta, and F. Greco (2003b), Bulk processes some months before the start of the 2001 Mt Etna eruption, evidenced throught microgravity studies, *J. Geoph. Res. 108*, No. B12, 2556.

Carbone, D., and F. Greco (2007), Review of Microgravity Observations at Mt. Etna: A Powerful Tool to Monitor and Study Active Volcanoes, *Pure Appl. Geophys. 164*, 1–22.

Carbone, D., G. Currenti, and C. Del Negro (2007), Elastic model for the gravity and elevation changes prior to the 2001 eruption of Etna volcano, *Bull. Volcanol. 69*, 553–562.

Carbone, D., G. Currenti, and C. Del Negro (2008), Multi-objective genetic algorithm inversion of ground deformation and gravity changes spanning the 1981 eruption of Etna volcano, *J. Geophys. Res.*, in press.

Carrozzo, M.T., R. de Franco, L. De Luca, D. Luzio, R. Primiceri, T. Quarta and M. Vitale (2002), Wavelet correlation filter for wide-angle seismic data, *Geoph. Prospect. 50*, n. 6, pp. 547-564.

Chiarabba, C., A. Amato, E. Boschi, and F. Barberi (1999), Recent seismicity and tomographic modeling of the Mount Etna plumbing system, *J. Geophys. Res. 105*, 10923-10938.

Clocchiatti , R., M. Condomines, N. Guènot, and J.C. Tanguy (2004), Magma changes at Mount Etna: the 2001 and 2002-2003 eruptions, *Earth Placet. Sci. Lett. 226*, 397-414.

Coifman, RR and M.V. Wickerhauser (1993), Wavelets and adapted waveform analysis. A toolkit for signal processing and numerical analysis, *Proceedings of Symposia in Applied Mathematics 47*, 119-145.

Continisio, R., F. Ferrucci, G. Gaudiosi, D. Lo Bascio, and G. Ventura (1997), Malta escarpment and Mt. Etna: early stages of an asymmetric rifting process? Evidences from geophysical and geological data, *Acta Vulcanol. 9 (1/2)*, 45-53.

Corsaro, R.A., and L. Miraglia (2004), Eruzione Etna 2004: Analisi petrografiche e composizionali preliminari, Inst. Naz. di Geofis. E Vulcanol., Catania, Italy, see http://www.ct.ingv.it/Report/RPTVGPTR20040927.pdf.

Corsaro, R.A. and M. Pompilio (2004), Magma dynamics in the shallow plumbing system of Mt.Etna as recorded by compositional variations in volcanics of recent summit activity (1995-1999), *J. Volcanol. Geotherm. Res. 137*,55-71.

Corsaro, R.A., L. Miraglia and M. Pompilio (2007), Petrologic evidence of a complex plumbing system feeding the July–August 2001 eruption of Mt. Etna, Sicily, Italy, *Bull Volcanol. 69*, 401–421 DOI 10.1007/s00445-006-0083-4.

Currenti, G., C. Del Negro, and G. Ganci (2007), Modelling of ground deformation and gravity fields using finite element method: An application to Etna volcano, *Geoph. J. Int. 169*, doi: 10.111/j.1365– 246X.2007.03380.x.

De Gori, P., Chiarabba C., and D. Patanè (2005), Qp structure of Mount Etna: Constraints for the physics of the plumbing system. *J. Geophys. Res.*, *110*, B05303, doi:10.1029/2003JB002875.

Farquharson, CG, and D.W. Oldenburg (2004), A comparison of automatic techniques for estimating the regularization parameters in non-linear inverse problems, *Geophys. J. Int. 156*, 411-425.

Fedi, M. and A. Rapolla (1999), 3-D inversion of gravity and magnetic data with depth resolution, *Geophysics 64*, 452-460.

Fedi, M. and G. Florio (2003), Decorrugation and removal of directional trends of magnetic fields by the wavelet transform: application to archaeological areas, *Geoph. Prospect. 51*, 261-272.

Fedi, M. and T. Quarta (1998), Wavelet analysis for the regional-residual and local separation of potential field anomalies, *Geoph. Prospect. 46*, 507-525.

Fedi, M., L. Lenarduzzi, R. Primiceri, and T. Quarta (2000), Localized Denoising Filtering Using the Wavelet Transform, *Pure Appl. Geophys. 157*, 1463–1491.

Fedi, M., R. Primiceri, T. Quarta, and V. Villani (2004), Joint application of continous and discrete wavelet transform on gravity data to identify shallow and deep sources, *Geophys. J. Int. 156*, 7-21.

Fedi, M., P.C Hansen, and V. Paoletti (2005), Analysis of depth resolution in potential field inversion, *Geophysics*, *70, 6*, A1-A11, doi:10.1190/1.2122408.

Ferrucci, F., R. Rasà, G. Gaudiosi, R. Azzaro, and S. Imposa (1993), Mt. Etna: a model for the 1989 eruption, *J. Volcanol. Geotherm. Res*. *56*, 35-56

Gill, P.E., W. Murray, D.B. Ponceleon, and M. Saunders (1991), Solving reduced KKT systems in barrier methods for linear and quadratic programming, *Technical Report*, SOL 91–7, Stanford University, Stanford, CA.

Greco, F., C. Carmisciano, C. Del Negro, I. Loretti, A. Sicali, and P. Stefanelli (2008), Seismic-induced accelerations detected by two coupled gravity meters in continuous recording with a high sampling rate at Etna volcano, *Annals of Geophysics*, *51*, 1.

Hinderer, J., and D. Crossley (2000), Time variations and inferences on the Earth's structure and dynamics, *Surv. Geophys. 21*, 1-45.

Houlie, N., P. Briole, A. Bonforte, and G. Puglisi (2006), Large scale ground deformation of Etna observed by GPS between 1994 and 2001, *Geophys. Res. Lett. 33*, L02309, doi:10.1029/2005GL024414.

La Delfa, S., V. Innocenti, G. Patanè, R. Clocchhiatti, J.L. Joron, and J.C. Tanguy (2001), Activity of Mount Etna precedine the February 1999 fissure eruption: inferred mechanism from seismological and geochemical data, *J. Volcanol. Geotherm. Res. 105*, 121-139.

Li, Y., and D.W. Oldenburg (1996), 3-D inversion of magnetic data, *Geophysics 61*, 394-408.

Métrich, N., P. Allard, N. Spilliaert, D. Andronico, and M. Burton (2004), 2001 flank eruption of the alkali- and volatile-rich primitive basalt responsible for Mount Etna's evolution in the last three decades, *Earth Planet Science Letter 228*, 1-17.

Moreau, F.D. Gibert, M. Holschneider, et al (1999), Identification of sources of potential fields with the continuous wavelet transform: Basic theory, *J. Geoph. Res. 104(B3)*, 5003–5013.

Murru, M., C. Montuori, M. Wyss, and E. Privitera (1999), The location of magma chambers at Mt. Etna, Italy, mapped by b-values, *Geophys. Res. Lett. 26*, 2553 – 2556.

Napoli, R., G. Currenti, and C. Del Negro (2007), Internal structure of Ustica volcanic complex (Italy) based on a 3D inversion of magnetic data, *Bulletin of Volcanology 69*, 869-879.

Neri, M., V. Acocella, and B. Behncke (2004), The role of the Pernicana Fault System in the spreading of Mount Etna (Italy) during the 2002-2003 eruption, *Bull. Volcanol. 66*, 417-430, DOI: 10.1007/s00445-003-0322-x.

Neri, M., V. Acocella, B. Behncke, V. Maiolino, A. Ursino, and R. Velardita (2005), Contrasting triggering mechanisms of the 2001 and 2002–2003 eruptions of Mount Etna (Italy), *J. Volcanol. Geotherm. Res. 144*, 235– 255.

Ogniben, L. (1966), Lineamenti idrogeologici dell'Etna, *Rivista Mineraria Siciliana 100-102*, 1-24.

Palano, M., G. Pugliesi, and S. Gresta (2007), Ground deformation at Mt. Etna: a joint interpretation of GPS and InSAR data from 1993 to 2000, *Bollettino di Geofisica Teorica ed Applicata 48*, 2, 81-98.

Patanè, D., O. Cocina, S. Falsaperla, E. Privitera, and S. Spampanato (2004), Mt. Etna: a seismological framework. in *Etna Volcano Laboratory*, Geophys. Monogr. Ser., vol. 143, edited

by A. Bonaccorso, S. Calvari, M. Coltelli, C. Del Negro and S. Falsaperla, pp. 147-165, AGU, Washington, D. C.

Patanè, D., E. Privitera, 2001. Seismicity related to 1989 and 1991-93 Mt. Etna (Italy) eruptions: kinematic constraints by fault solution analysis. J. Volcanol. Geotherm. Res., 109, 77 – 98.

Patanè, D., P. De Gori, C. Chiarabba, and A. Bonaccorso (2003), Magma ascent and the pressurization of Mount Etna's volcanic system, *Science*.

Puglisi, G. and A. Bonforte (2004), A. Dynamics of Mount Etna Volcano inferred from static and kinematic GPS measurements, *J. Geophys. Res. 109*, 1-15.

Regione Siciliana - SIAS - *Servizio Informativo Agrometeorologico Siciliano*.

Romano, R. (1982), Geological map of Mt. Etna, *Progetto Finalizzato Geodinamica*, Istituto Internazionale di Vulcanologia, Catania, 1:50.000 scale.

Rust, D., B. Behncke, M. Neri, and A. Ciocanel (2005), Nested zones of instability in the Mount Etna volcanic edifice, Sicily, *J. Volcanol. Geotherm. Res. 144*, 137-153, doi: 10.1016/j.jvolgeores.2004.11.021.

Schiavone, D., and M. Loddo (2007), 3-D density model of Mt. Etna Volcano (Southern Italy), *J. Volcanol. Geoth. Res. 164*, 161–175.

Tibaldi, A. and G. Groppelli (2002), Volcano-tectonic activity along structures of the unstable NE flank of Mt. Etna (Italy) and their possible origin, *J. Volcanol. Geotherm. Res. 115*, 277-302.

Table 1

Wavelet Basis	Shannon's Entropy
Coiflet 2	3.24
Coiflet 3	3.97
Coiflet 4	4.50
Daubechies 1	4.38
Daubechies 2	3.60
Daubechies 3	4.02
Daubechies 4	3.20
Symmlet 1	4.38
Symmlet 2	3.60
Symmlet 3	4.02
Symmlet 4	**3.14**
Symmlet 5	3.55
Symmlet 6	3.83
Symmlet 7	3.81

Table 1 - Shannon's entropy values relative to wavelet basis. The minimum entropy values is obtained using Symlet 4 bases.

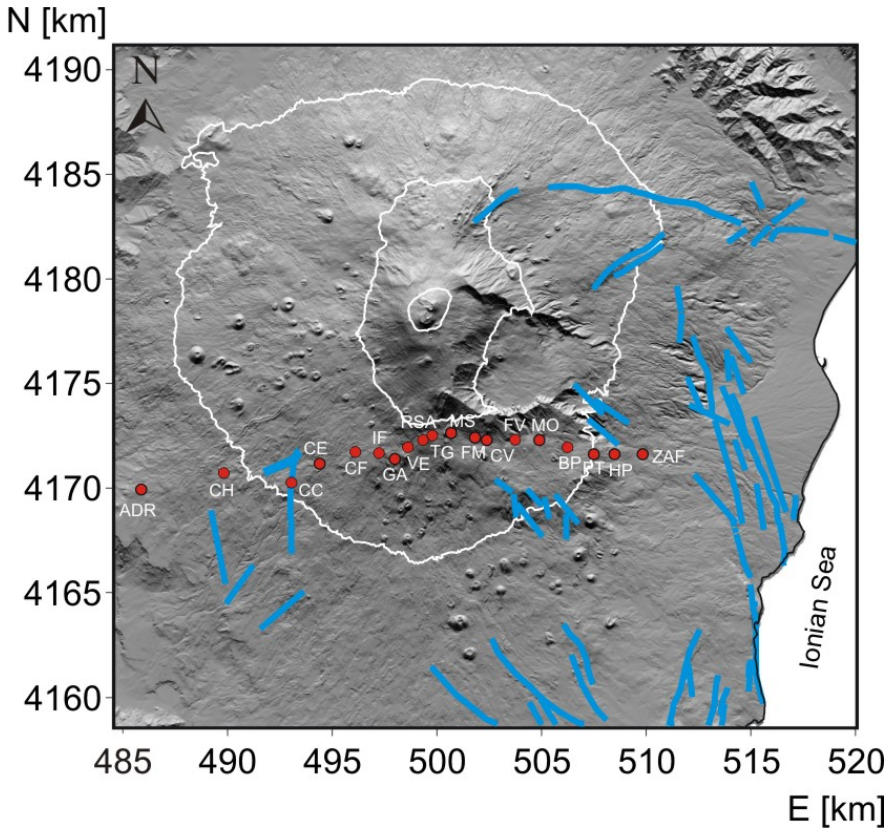

Fig. 1 – Sketch map of Mt. Etna showing the gravity stations (red circles) that compose the East – West profile on the southern slope of the volcano which runs from Zafferana to Adrano across the Rifugio Sapienza. The blue lines show the major surface fault systems bordering the eastern and southern sectors of the volcano. Geographical coordinates are expressed in UTM projection, zone 33N.

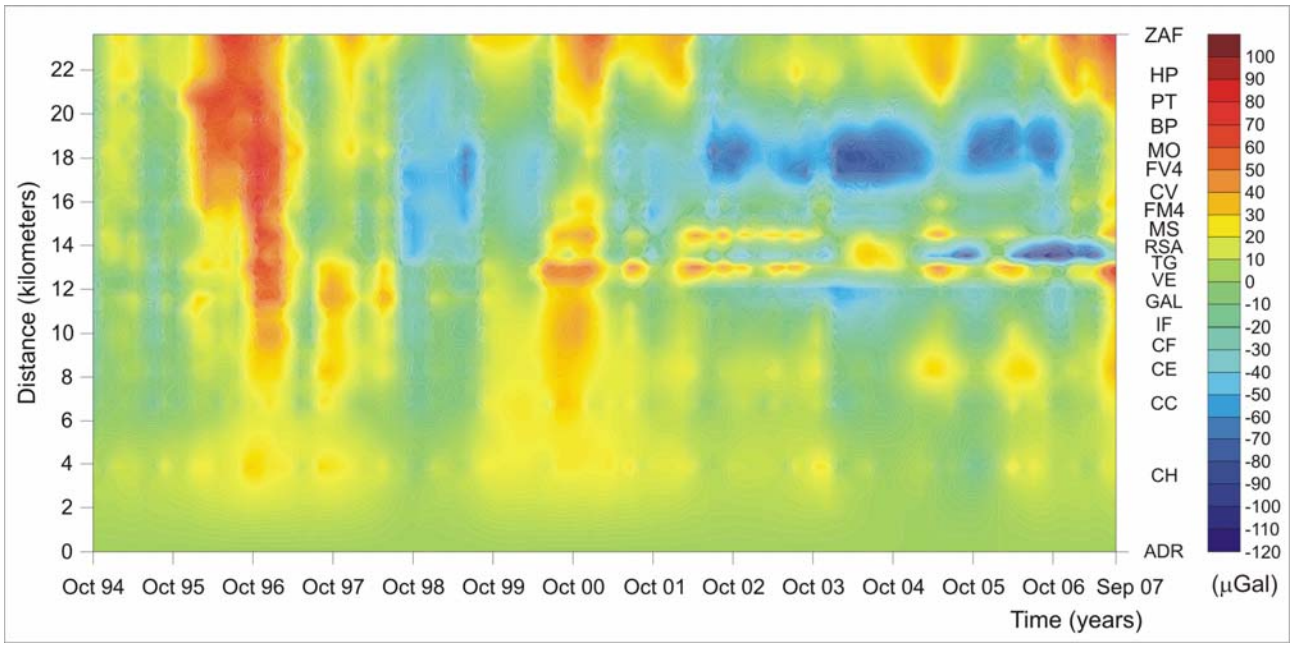

Fig. 2 - Image showing the space/time gravity variations along a 24-kilometer East – West trending profile of 19 stations between October 1994 and September 2007. All measurements were referred to the outermost station of the profile (Adrano; ADR). The error on temporal gravity differences along the East-West profile is 10 μGal.

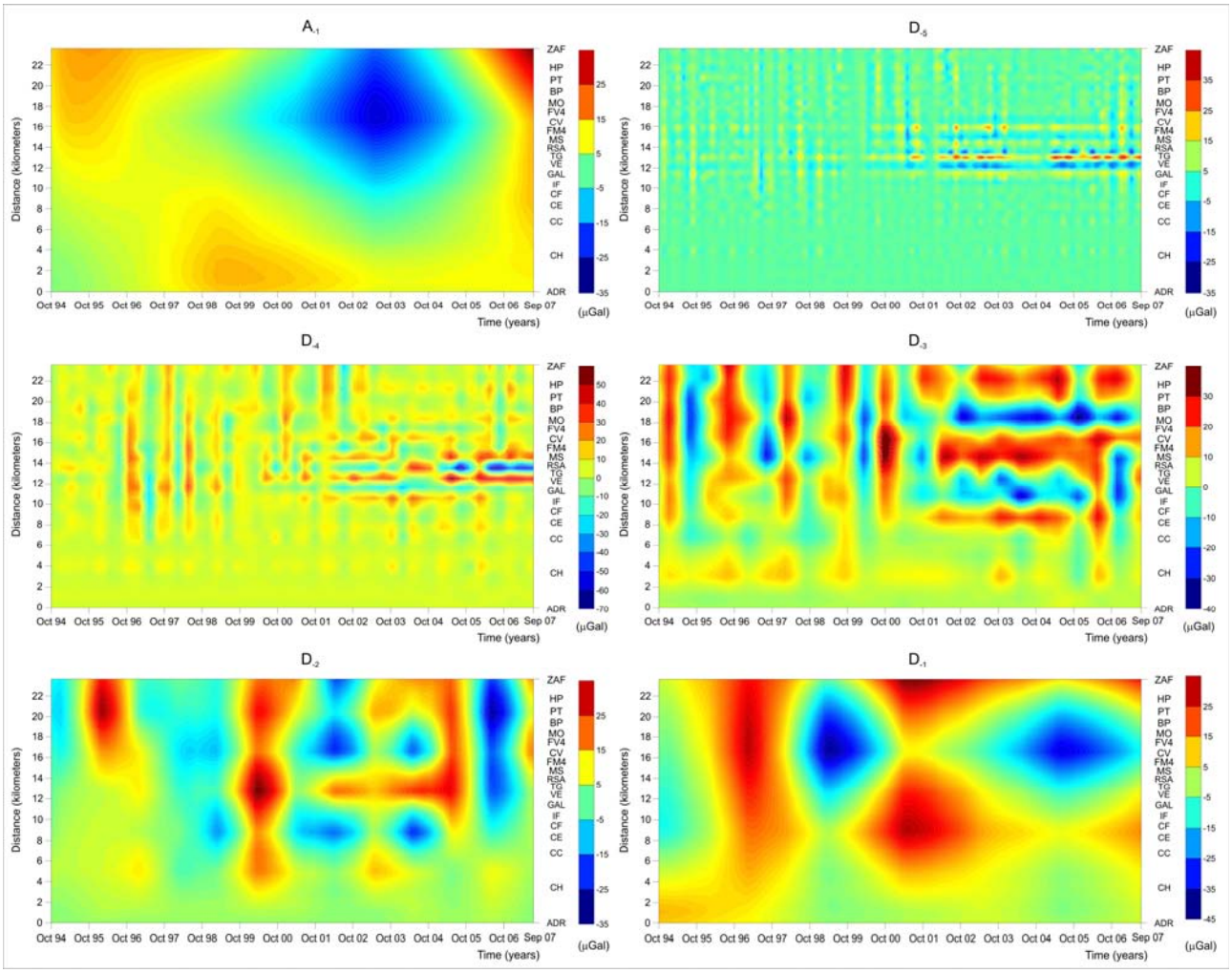

Fig. 3 – Wavelet multiresolution analysis of the 14-year-long gravity data-set. Using a Symlet 4 wavelet base, five total detail maps and a low resolution map (A_1) were obtained. The meaningful gravity anomalies are related to the total detail levels from D_{-3} to D_{-1}.

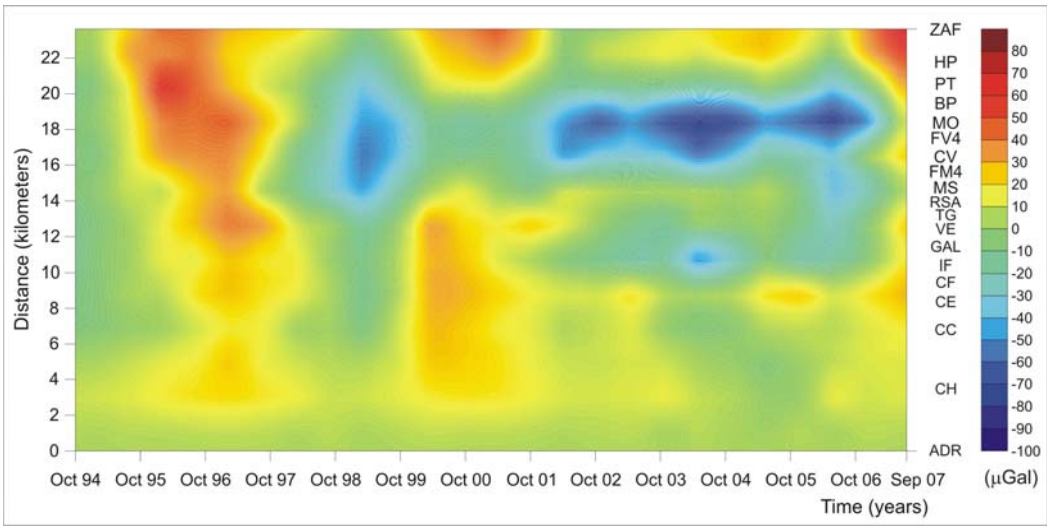

Fig. 4 – The 14-year-long gravity data-set after filtering the contributions identified in the D_{-5} and D_{-4} total maps and the D_{-3} vertical detail.

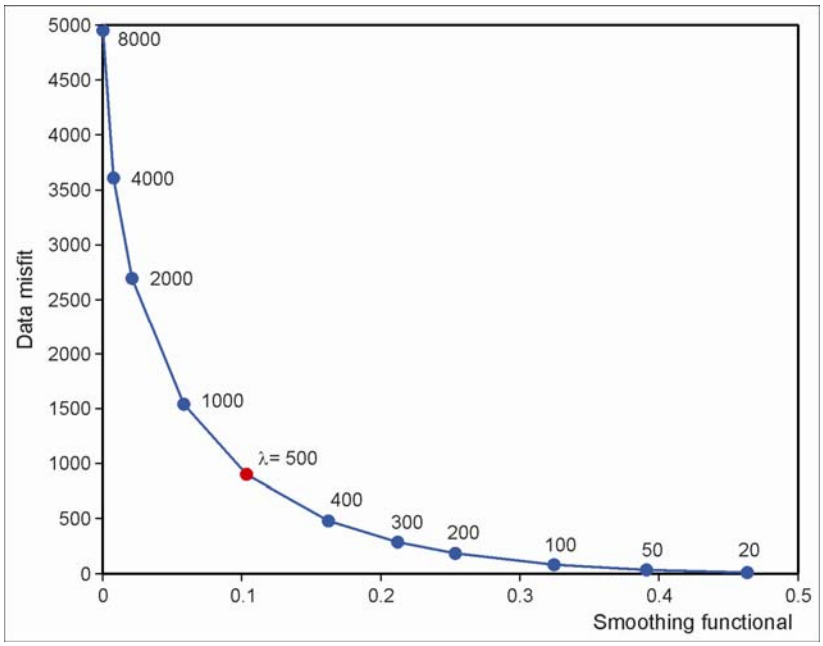

Fig. 5 – The L-curves of the data misfit versus the smoothing functional as a function of the regularization parameter. The point of maximum curvature lies on a corresponding value of λ = 500.

.

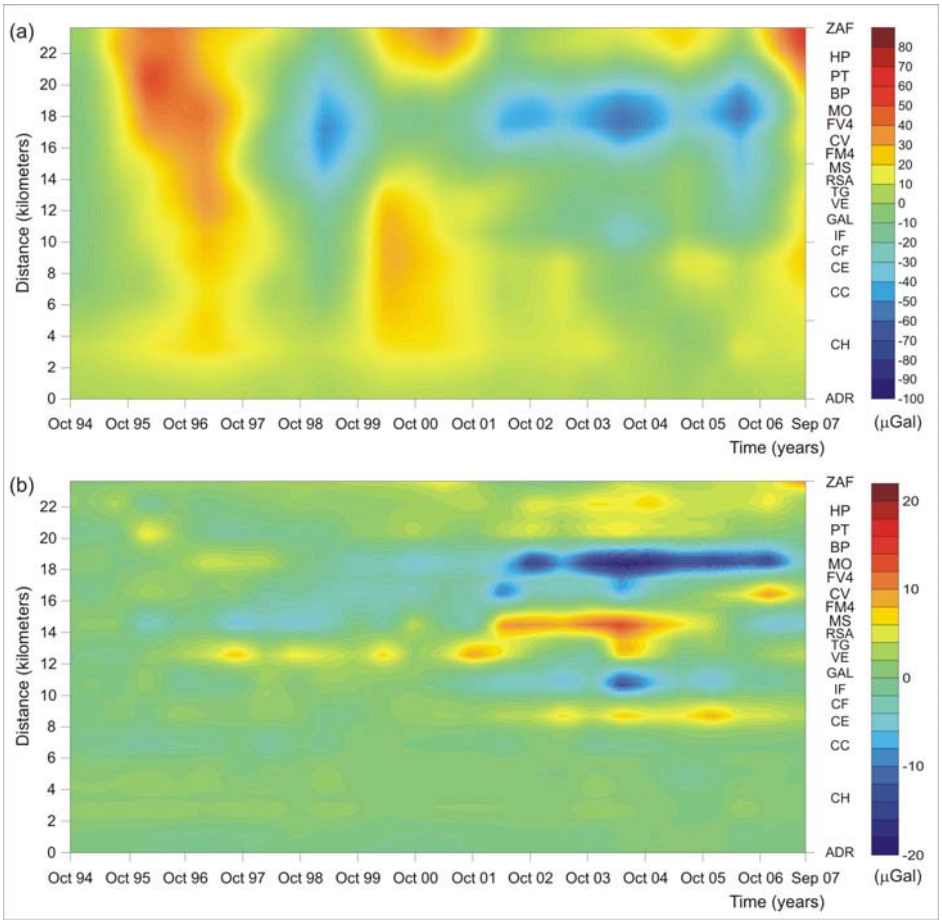

Fig. 6 – Computed gravity anomaly map related to the value of λ = 500 (a) and residual gravity anomaly map (b).

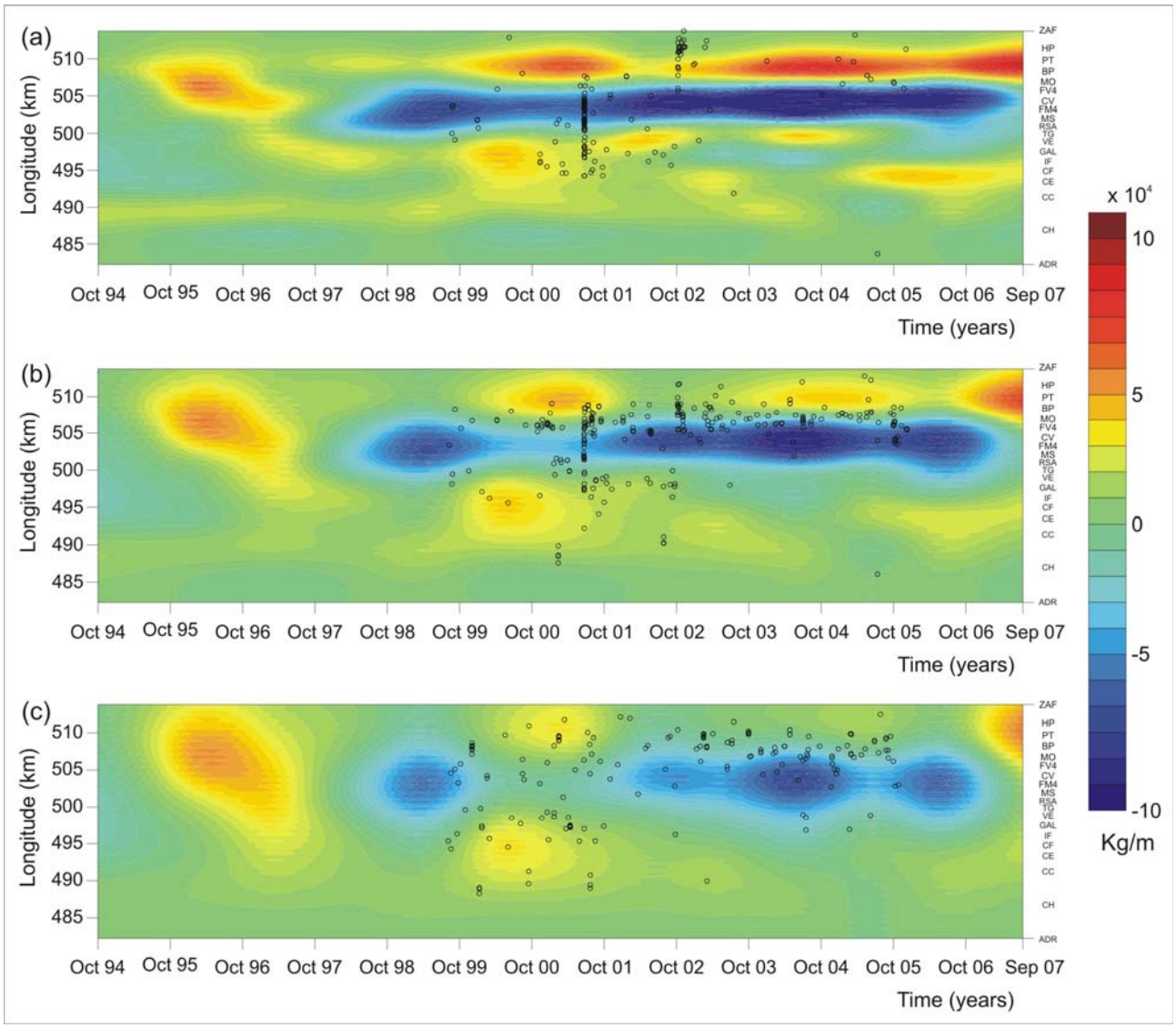

Fig. 7 – Maps of the 2D recovered density model (Kg/m) at three different depths: -1 km (a); – 3km (b); – 6 km (c). A comparison with the hypocentral depths (-1km ±1; -3km ±1; -6 km±1) of seismic events (white circles) clustered during August 1999 – January 2006 period, is also reported.

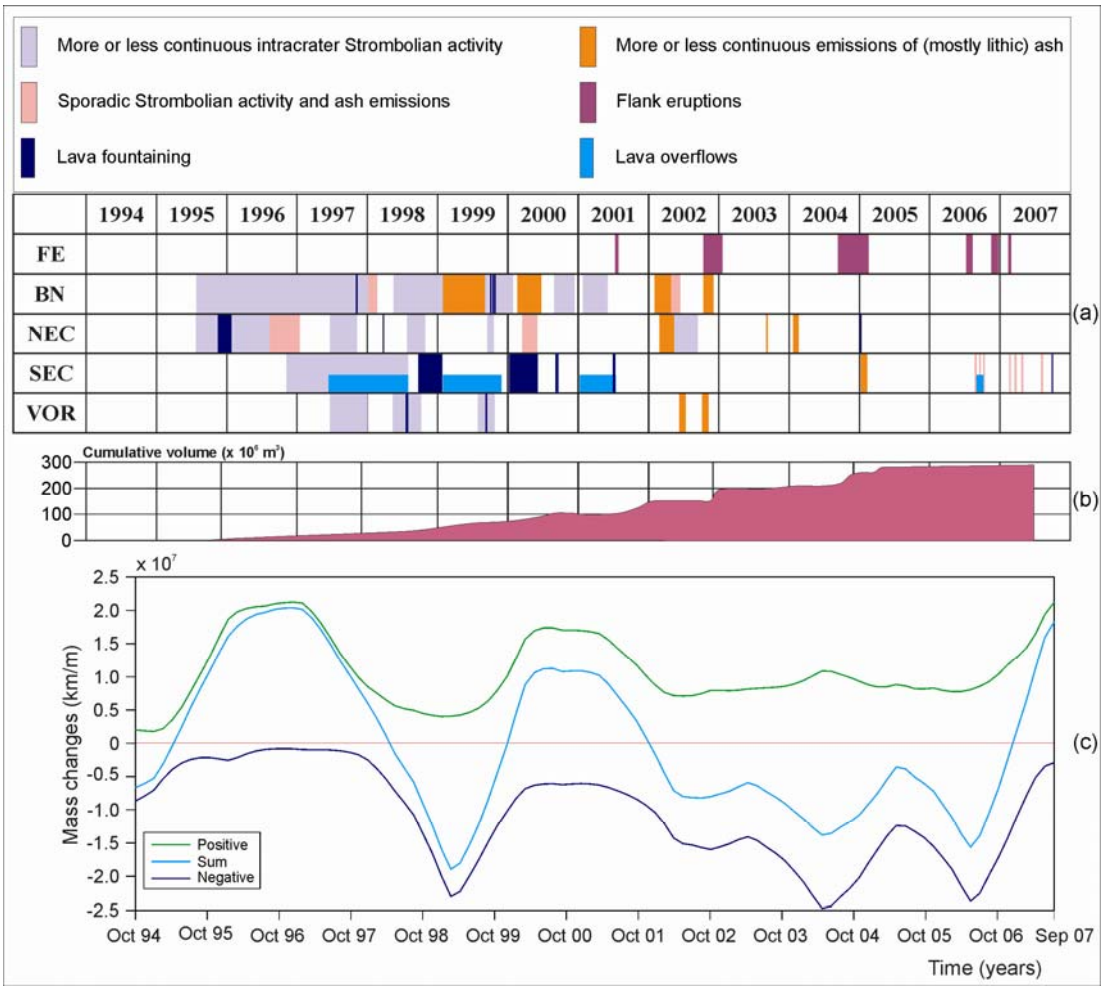

Fig. 8 – The 1994 – 2007 timeline showing: (a) different eruptive styles (after *Allard et al*., [2006]) for flank eruptions (FE) and for the four summit craters (Bocca Nuova BN; Northeast Crater NE; Southeast Crater SEC; Voragine VOR;); (b) cumulative eruptive volume redrawn from *Allard et al.*, [2006] (expressed as dense rock equivalent); (c) mass change per unity length computed beneath the profile discriminating the density variation of prisms: positive values (green), negative values (blue), and both positive and negative values (cyan).